AGU ADVANCING EARTH AND SPACE SCIENCES

Geophysical Research Letters®

RESEARCH LETTER
10.1029/2024GL112619

# Is There a Scalar Atmospheric Surface Layer Within a Convective Boundary Layer? Implications for Flux Measurements

**Heping Liu[1], Cheng Liu[2], Yanzhao Zhou[3], Qianyu Zhang[1], Ankur R. Desai[4], Khaled Ghannam[5], Jianping Huang[6], and Gabriel G. Katul[7]**

[1]Department of Civil and Environmental Engineering, Washington State University, Pullman, WA, USA, [2]Jiangxi Provincial Key Laboratory of Genesis and Remediation of Groundwater Pollution/School of Water Resources and Environmental Engineering, East China University of Technology, Nanchang, China, [3]School of Geographical Sciences/Hebei Technology Innovation Center for Remote Sensing Identification of Environmental Change/Hebei Key Laboratory of Environmental Change and Ecological Construction, Hebei Normal University, Shijiazhuang, China, [4]Department of Atmospheric and Oceanic Sciences, University of Wisconsin-Madison, Madison, WI, USA, [5]Department of Civil and Environmental Engineering, Northeastern University, Boston, MA, USA, [6]Environmental Modeling Center, NOAA National Centers for Environmental Prediction, College Park, MD, USA, [7]Department of Civil and Environmental Engineering, Duke University, Durham, NC, USA

**Abstract** Top-down entrainment shapes the vertical gradients of sensible heat, latent heat, and $CO_2$ fluxes, influencing the interpretation of eddy covariance (EC) measurements in the unstable atmospheric surface layer (ASL). Using large eddy simulations for convective boundary layer flows, we demonstrate that decreased temperature gradients across the entrainment zone increase entrainment fluxes by enhancing the entrainment velocity, amplifying the asymmetry between top-down and bottom-up flux contributions. These changes alter scalar flux profiles, causing flux divergence or convergence and leading to the breakdown of the constant flux layer assumption (CFLA) in the ASL. As a result, EC-measured fluxes either underestimate or overestimate "true" surface fluxes during divergence or convergence phases, contributing to energy balance non-closure. The varying degrees of the CFLA breakdown are a fundamental cause for the non-closure issue. These findings highlight the underappreciated role of entrainment in interpreting EC fluxes, addressing non-closure, and understanding site-to-site variability in flux measurements.

**Plain Language Summary** In the atmosphere over a heated surface, water vapor, carbon dioxide, and heat are transported from both the ground (bottom-up) and the top of the air column (top-down). The swirling motion of air within the column helps to even out the distribution of these quantities, known as "scalars." Scalar fluxes measure how many molecules of these substances cross a unit area over time. At the surface, energy balance and plant processes control heat, water vapor, and carbon dioxide fluxes. However, fluxes at the top of the air column do not follow the same rules and abide by the same constraints as their ground counterpart. This study uses numerical simulations to show that when the temperature difference across a layer at the top of the boundary layer decreases, the boundary layer becomes deeper, increasing the transport of heat from the top. This causes changes in the slopes of flux profiles, disrupting the assumption that fluxes remain constant with height even close to the ground surface. As a result, measurements near the surface often underestimate or overestimate true surface fluxes, contributing to the much-debated surface energy balance non-closure problem.

**Key Points:**

- Entrainment-modulated top-down transport influences the slopes of the scalar flux profiles in the unstable atmospheric surface layer
- Variations in scalar flux profiles lead to differing degrees of failure in the constant flux layer assumption (CFLA) for different scalars
- The failure of the CFLA explains the non-closure issue in the surface energy balance

**Supporting Information:**

Supporting Information may be found in the online version of this article.

**Correspondence to:**

H. Liu,
heping.liu@wsu.edu

**Citation:**

Liu, H., Liu, C., Zhou, Y., Zhang, Q., Desai, A. R., Ghannam, K., et al. (2025). Is there a scalar atmospheric surface layer within a convective boundary layer? Implications for flux measurements. *Geophysical Research Letters*, *52*, e2024GL112619. https://doi.org/10.1029/2024GL112619

Received 18 SEP 2024
Accepted 11 FEB 2025



## 1. Introduction

It is widely recognized that the exchange of scalars such as heat, water vapor, and $CO_2$ across the land-atmosphere interface is of significance to numerous applications. These scalar fluxes are typically measured by eddy covariance (EC) systems in the atmospheric surface layer (ASL) and are presumed to represent the true fluxes across the land-atmosphere interface (Butterworth et al., 2021). This approach relies on the so-called constant flux layer assumption (hereafter the CFLA) that also forms the basis of Monin-Obukhov similarity theory (MOST) (Stull, 1988; Wyngaard, 2010). However, the widely reported non-closure of the surface energy balance (hereafter non-closure) suggests that sensible (*SH*) and latent (*LH*) heat fluxes measured by EC systems in the ASL may be underestimated, or in some cases, overestimated compared to the respective true fluxes exchanged at the

land-atmosphere interface (Gao et al., 2018; Mauder et al., 2020; Oncley et al., 2007; Stoy et al., 2013). Increasing evidence from EC data and large eddy simulations (LES) points to large turbulent eddies associated with boundary-layer processes as a major cause of the non-closure (Foken et al., 2011; Gao et al., 2017; H. Liu, Gao, & Katul, 2021; Liu, Liu, Huang, et al., 2024; Wanner et al., 2024). The extent to which changes in boundary-layer processes regulate the influence of large turbulent eddies on scalar fluxes and their profiles as well as turbulence statistics in the unstable ASL is now receiving increased interest and scrutiny (Cava et al., 2006; Cancelli et al., 2014; D. Li et al., 2018; Q. Li et al., 2018; C. Liu, Liu, et al., 2021; H. Liu, Gao, & Katul, 2021; Liu, Liu, Huang, et al., 2024).

At the surface, energy balance and plant related processes govern heat, water vapor, and $CO_2$ fluxes, but at the top of the boundary layer, these fluxes follow different rules and constraints. In the convective boundary layer (CBL), buoyancy-driven large turbulent eddies, termed as ejections, rise from the surface, overshoot the capping inversion, and cause the entrainment of stably stratified air from the free atmosphere into the boundary layer as descending large eddies, or sweeps (Conzemius & Fedorovich, 2006; Stull, 1988; Wyngaard, 1982). These top-down large eddies with entrained air masses can travel across the CBL and impinge into the ASL, as indicated by observed negative skewness profiles of a trace gas (Lanotte & Mazzitelli, 2013). These top-down processes through sweeps affect momentum and scalar fluxes in the ASL (Katul et al., 1997), causing deviations of turbulence statistics from their classic MOST scaling (Khanna & Brasseur, 1997; Q. Li et al., 2018; Wyngaard, 1982). Moreover, they cause breakdown in gradient-diffusion closure relations (Ghannam et al., 2017), the ASL temperature-humidity dissimilarity (Cancelli et al., 2014; Gao et al., 2018; C. Liu, Liu, et al., 2021), increased flux divergence and convergence (Gao et al., 2016), and decreased flux transport efficiencies for water vapor and $CO_2$ (Liu, Liu, Huang, et al., 2024). Flux divergence and convergence, observed by turbulent flux measurements (Gao et al., 2016; Mahrt et al., 2021; Ortiz-Suslow et al., 2021), indicate that fluxes measured in the ASL can be biased compared to the true surface interfacial fluxes depending on the interplay between the entrainment processes and the ability of large eddies to propagate these entrainment effects into the ASL.

Vertical transport of scalars at any level $z$ from the ground surface can be treated as a superposition of bottom-up processes from the surface and top-down processes from the entrainment zone, resulting in a linear height-dependence of scalar fluxes or changes in slopes of flux profiles (Sorbjan, 1999; Wyngaard, 1990; Wyngaard & Brost, 1984). Changes in the slopes of flux profiles in the CBL (i.e., changes in flux divergence and convergence) are also linked to variations in asymmetric contributions between top-down entrainment fluxes and bottom-up surface interfacial fluxes of the corresponding scalars (Liu, Liu, Huang, et al., 2024). While these previous studies focused on how changes in bottom-up processes affect ASL flux divergence and convergence through altering the surface Bowen ratio (e.g., Liu, Liu, Huang, et al., 2024), the influence of changes in top-down processes on flux divergence and convergence in the ASL remains less explored and frames the scope here.

Entrainment-induced fluxes into the boundary layer can act as a source or sink of scalars, depending on the scalar increment across the capping inversion (Lanotte & Mazzitelli, 2013). However, what has been less explored is how changes in the mean temperature gradient across the entrainment (EZTG) zone (EZTG) modify bottom-up buoyancy-driven boundary layer growth into the capping inversion. This in turn alters entrainment-induced top-down fluxes and the asymmetric flux transport by sweeps and ejections, leading to changes in the slopes of scalar flux profiles. Additionally, the implications of these changes in the slopes for the validity of the CFLA and how this assumption's failure contributes to the non-closure issue is incomplete and requires further investigation.

To address these questions, a series of LES experiments are conducted for horizontally homogeneous, quasi-stationary flows in the CBL with three different temperature gradient values across the entrainment zone. The model domain is flat and covered with uniform short grass under three varying soil moisture conditions. This study specifically targets CBL flows due to the observed increase in the non-closure under conditions of increasing instability in the CBL (Stoy et al., 2013; H. Liu, Gao, & Katul, 2021; Zhou et al., 2018). Here, the non-closure is assessed by the closure ratio. As outlined in Liu, Liu, Huang, et al. (2024), non-closure manifests when the closure ratio, defined as $CR = \frac{SH+LH}{SH_0+LH_0}$, deviates from unity. Here $(SH + LH)$ represents the sum of the measured $SH$ and $LH$ at any height in the ASL, as reported by EC systems, while $(SH_0 + LH_0)$ is the sum of their "true" surface fluxes, balanced by the surface available energy (i.e., $SH_0 + LH_0 = Rn_0 - G_0$, where $Rn_0$ is the surface net radiation and $G_0$ is the ground heat flux).

## 2. LES Model and Configurations

The National Center for Atmospheric Research LES model (Moeng, 1984; Patton et al., 2005; Sullivan et al., 1996), coupled with a land-surface model (LSM) (Huang et al., 2009), is employed to address the study objectives. The LSM provides surface fluxes of sensible and latent heat and $CO_2$, consistent with previous studies (e.g., Huang et al., 2009; Liu, Liu, Huang, et al., 2024). The LSM computes surface sensible and latent heat fluxes in a manner that guarantees surface energy-balance closure. The governing equations and main features of the LES model are detailed in Moeng (1984). The simulation domain is $5.0 \times 5.0 \times 1.92$ km with a grid spacing of $10 \times 10 \times 4$ m resulting in $500 \times 500 \times 480$ grid points in the $x$ (longitudinal), $y$ (lateral), and $z$ (vertical) directions, respectively. This setup, similar to C. Liu, Liu, et al. (2021), is sufficient to resolve key turbulence features in the CBL (e.g., C. Liu, Liu, et al., 2021; Liu, Liu, Huang, et al., 2024). The ground is represented by grassland with a momentum roughness length of 0.1 m and an albedo of 0.2.

To evaluate the effects of varying entrainment fluxes on scalar transport in the ASL, three sets of simulations are performed with three temperature gradient values of 0.05, 0.1, and 0.2 K/m across the entrainment zone. These three temperature gradient regimes represent weak (EZweak), moderate (EZmoderate), and strong EZTG (EZstrong) conditions (Table S1 in Supporting Information S1). These choices are typical of atmospheric conditions (e.g., Sorbjan, 2005). Additionally, simulations are run for three soil moisture conditions as measured by a soil saturation factor ($f_n$): dry ($f_n = 0.05$), moderate dry ($f_n = 0.3$), and wet ($f_n = 0.9$) soils, resulting in nine cases (Table S1 in Supporting Information S1). A constant incident solar radiation of 700 W $m^{-2}$ is prescribed, and geostrophic wind forcing is assumed to be zero, representing a shear-free CBL.

The initial profiles of potential temperature ($\theta$), specific humidity ($q$), and $CO_2$ mixing ratio ($C$) are provided in Figures 1a, 1b, and 1c. Specifically, $\theta$ is constant at 290 K within the mixed layer of height $z_i$ with a gradient of 0.006 K $m^{-1}$ in the free atmosphere, and three varying gradients in the entrainment zone. The $q$ profile is constant at 8 g $kg^{-1}$ in the mixed layer, decreases at $-0.175$ g $kg^{-1}$ $m^{-1}$ in the interfacial layer, and remains constant at 1 g $kg^{-1}$ in the free atmosphere. The $C$ profile has a constant value of 531 mg $kg^{-1}$ within the mixed layer, a positive gradient of 0.75 mg $kg^{-1}$ $m^{-1}$ in the interfacial layer, and a constant value of 561 mg $kg^{-1}$ above it similar to Huang et al. (2009). Each simulation's timestep is dynamically adjusted to satisfy the Courant, Friedrichs, and Lewy conditions. Idealized horizontal periodic boundary conditions are applied throughout the simulations. Sensitivity tests confirm that the results are not influenced by variations in domain height, domain size, or horizontal grid spacing (Figures S1, S2, and S3 in Supporting Information S1). The LES analysis is based on 1 hr averages after the domain-averaged turbulence kinetic energy reaches a stationary state (Figure S4 in Supporting Information S1). The 1 hr averages ensure multiple eddy turn-over time to be interrogated in turbulent flux calculations.

## 3. Results and Discussion

### 3.1. EZTG-Induced Changes in Entrainment Fluxes Under Three Soil Moisture Conditions

Figures 1d, 1e, and 1f present normalized fluxes of kinematic sensible heat $\left(\overline{w'\theta'}/\overline{w'\theta'}_0\right)$, water vapor $\left(\overline{w'q'}/\overline{w'q'}_0\right)$, and $CO_2$ $\left(\overline{w'C'}/\overline{w'C'}_0\right)$ for the three EZTG settings across the three soil moisture conditions. These fluxes are domain-averaged horizontally after time-averaging at each grid point. Under the three EZTG conditions, $\overline{w'\theta'}/\overline{w'\theta'}_0$ always decreases linearly with $\frac{z}{z_i}$ across the three soil moisture conditions (i.e., flux divergence) (Figure 1d). However, $\overline{w'q'}/\overline{w'q'}_0$ shows a linear decrease with $\frac{z}{z_i}$ for EZstrong-M and EZstrong-W (i.e., flux divergence) but a linear increase with $\frac{z}{z_i}$ (i.e., flux convergence) for other cases (Figure 1e). Most cases exhibit a linear decrease in $\overline{w'C'}/\overline{w'C'}_0$ with $\frac{z}{z_i}$ (i.e., flux divergence), except EZweak-D, EZmoderate-D, and EZweak-M, which show flux convergence (Figure 1f). These linear dependences for $\overline{w'\theta'}/\overline{w'\theta'}_0$, $\overline{w'q'}/\overline{w'q'}_0$, and $\overline{w'C'}/\overline{w'C'}_0$ on $\frac{z}{z_i}$ have been reported elsewhere (Andre et al., 1978; Ek & Holtslag, 2004; Ghannam et al., 2017; Huang et al., 2008, 2009, 2011; Lanotte & Mazzitelli, 2013; Liu, Liu, Huang, et al., 2024; Mellado et al., 2017; Stull, 1988). To explain this linearity, the mean conservation equation for an arbitrary scalar $s$ at high Reynolds number is considered, where molecular diffusion is negligible compared to turbulent transport, under horizontally homogeneous conditions and with no subsidence. This yields:

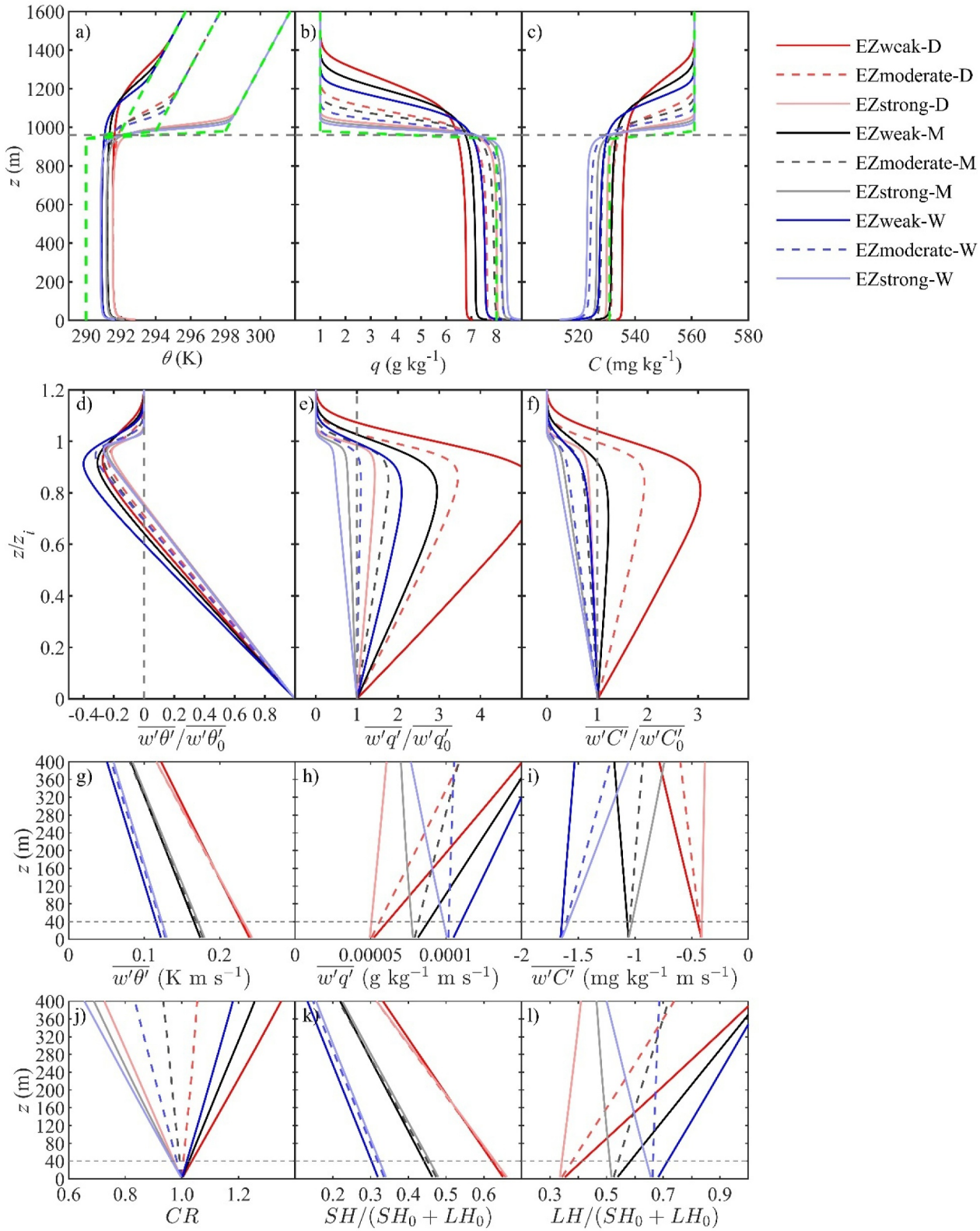


**Figure 1.**

$$\frac{\partial \overline{S}}{\partial t} = -\frac{\partial \overline{w's'}}{\partial z}, \tag{1}$$

where $t$ is time, $\overline{S}$ is the mean scalar concentration, $\overline{w's'}$ is the vertical turbulent flux, and $z$ is, as before, the vertical coordinate. Differentiating with respect to $z$ gives:

$$\frac{\partial}{\partial t}\left(\frac{\partial \overline{S}}{\partial z}\right) = -\frac{\partial^2 \overline{w's'}}{\partial z^2}. \tag{2}$$

In the CBL, assuming a well-mixed mean scalar concentration (i.e., $\frac{\partial \overline{S}}{\partial z} = 0$), and integrating twice with respect to $z$ gives (Huang et al., 2008; Sorbjan, 1999; Wyngaard & Brost, 1984):

$$\frac{\overline{w's'(z)}}{\overline{w's'}_0} = 1 - (1-\alpha)\left(\frac{z}{z_i}\right), \tag{3}$$

where $\alpha = \frac{\overline{w's'}_{z_i}}{\overline{w's'}_o}$ is the entrainment ratio, $\overline{w's'}_o$ is the "true" surface flux, and $\overline{w's'}_{z_i}$ is the flux at the boundary layer top $z_i$ impacted by entrainment. In the ASL, it is commonly assumed that $\frac{z}{z_i} \ll 1$. This assumption is the essence of MOST that argues turbulent fluxes at any $z$ closely approximate the true ground fluxes near the ground. However, there are cases where $\frac{z}{z_i} \sim 0.1$ and $\alpha$ exceeds two causing significant deviations between the ASL turbulent flux and surface flux. This situation becomes significantly amplified and problematic when $\alpha < 0$. Linear dependence of $\overline{w's'}(z)$ on $z$ occurs when the "storage term" at any $z$ (i.e., $\frac{\partial \overline{S}}{\partial t}$) is retained. It is the well-mixed condition that eliminates its contribution from the mean scalar continuity equation upon vertical differentiation.

Returning to the entrainment fluxes, a model for the entrainment of heat or scalar fluxes at $z = z_i$ is given by $F_i = -\mu w_e(\Delta_{EZ}s)$, where $\Delta_{EZ}s$ is the EZTG or passive scalar increment across the entrainment zone, $w_e$ is the entrainment velocity (Lanotte & Mazzitelli, 2013), and $\mu$ is an empirical constant. The $w_e$ is assumed to be proportional to the convective velocity $w_* = \left(\frac{gz_iH_0}{\theta_0}\right)^{\frac{1}{3}}$ and the inverse bulk Richardson number $Ri^* = gz_i\Delta_{EZ}\theta/(\theta_0 w_*^2)$. This assumption implies that in a shear-free CBL, turbulent processes in the entrainment zone are directly related to surface heating (i.e., $H_0$). Therefore, $w_e$ and $\Delta_{EZ}s$ are the major factors accounting for the influences of varying entrainment processes on entrainment fluxes in a shear-free CBL (Lanotte & Mazzitelli, 2013).

Under fixed soil moisture conditions with an almost constant $\overline{w'\theta'}_0$, vertical motion is largely enhanced as the EZTG decreases, leading to the increased $w_*$ due to the reduced stability across the entrainment zone (Table S2 in Supporting Information S1). Both $w_e$ and $z_i$ also increase as the EZTG decreases. Despite the decreased EZTG, the entrainment heat flux (i.e., $\overline{w'\theta'}_{z_i}$) increases primarily due to the enhanced $w_e$. Correspondingly, the entrainment ratio for heat flux ($\alpha_{SH}$) becomes more negative, ranging from −0.40 to −0.22. Once buoyancy-induced vertical motions primarily driven by $\overline{w'\theta'}_0$ are established (as quantified by $w_*$ and $w_e$) in the CBL, the top-down fluxes of $H_2O$ and $CO_2$ (i.e., $\overline{w'q'}_{z_i}$ and $\overline{w'C'}_{z_i}$) are dependent upon $\Delta_{EZ}s$. Under fixed soil moisture conditions, there are almost unvarying $\overline{w'q'}_0$ and $\overline{w'C'}_0$ that represent the unvarying bottom-up forcing. As $w_e$ increases with decreasing EZTG, $\overline{w'q'}_{z_i}$ and $\overline{w'C'}_{z_i}$ increase accordingly, leading to a corresponding increase in

**Figure 1.** Profiles of (a) potential temperature ($\theta$), (b) specific humidity ($q$), (c) $CO_2$ concentration ($C$), (d) normalized kinematic heat flux ($\overline{w'\theta'}/\overline{w'\theta'}_0$), (e) water vapor flux ($\overline{w'q'}/\overline{w'q'}_0$), (f) $CO_2$ flux ($\overline{w'C'}/\overline{w'C'}_0$) in the convective boundary layer (CBL). Note that both $\overline{w'C'}$ at any height in the CBL and $\overline{w'C'}_0$ are negative for the nine cases in the model domain covered with grass, making the $\overline{w'C'}/\overline{w'C'}_0$ values positive through the CBL. The green dash lines in (a), (b), and (c) are initial profiles. The gray dash line is the initial boundary-layer height (960 m). Profiles of (g) kinematic heat flux ($\overline{w'\theta'}$), (h) water vapor flux ($\overline{w'q'}$), (i) $CO_2$ flux ($\overline{w'C'}$), (j) the closure ratio of the energy balance: $CR = (SH + LH)/(SH_0 + LH_0)$, (k) $SH/(SH_0 + LH_0)$, and (l) $LH/(SH_0 + LH_0)$ below $z < 400$ m. Note that $SH/(SH_0 + LH_0)$ denotes the contribution of sensible heat flux ($SH$) to $CR$, and $LH/(SH_0 + LH_0)$ denotes the contribution of latent heat flux ($LH$) to $CR$. Subscript "0" denotes the surface value. The results shown in this figure are based on the domain-averaged fluxes.

the entrainment ratio for $LH$ ($\alpha_{LH}$) and $F_c$ ($\alpha_{F_c}$) that range from 0.44 to 5.34 and 0.12 to 3.05, respectively (Table S2 in Supporting Information S1).

Under fixed $f_n$, $\beta$ is constant over hourly averaging periods. The progressively enhanced top-down transfer by large eddies with decreasing EZTG becomes evident by the gradually increased negative vertical velocity across the CBL, particularly in its upper part (Figure S5 in Supporting Information S1). These strengthened sweeping eddies lead to enhanced downward impingement on the ASL from the mixed layer, regulating turbulent scalar flux gradients in the ASL. Consequently, such increased entrainment fluxes contribute to the increased asymmetry in flux contributions by sweeps and ejections across the CBL, eroding the ASL by enforcing a well-mixed state as EZTG increases. Under fixed soil moisture conditions, EZTG-induced changes in $\alpha_{SH}$, $\alpha_{LH}$ and $\alpha_{F_c}$ range from 10.1% to 24.5%, 54.6% to 147.3%, and 57.4% to 183.7%, respectively (Table S2 in Supporting Information S1). These entrainment ratios more than compensate for the small $z/z_i$ in the mean continuity equation when applied to the ASL.

As $f_n$ increases (i.e., decreasing $\beta$), more available energy is partitioned into $LH_0$ (i.e., increasing $\overline{w'q'}_0$) reducing $\overline{w'\theta'}_0$ and making $\overline{w'C'}_0$ more negative due to the enhanced $CO_2$ uptake accompanying the larger transpiration rate. Under fixed EZTG conditions, the decreased $\overline{w'\theta'}_0$ reduces $w_*$ and $w_e$ with increasing soil moisture, decreasing $\overline{w'\theta'}_{z_i}$, $\overline{w'q'}_{z_i}$, and $\overline{w'C'}_{z_i}$ (Table S2 in Supporting Information S1). Consequently, $\alpha_{SH}$ increases in wetter cases, primarily due to the larger reduction in $\overline{w'\theta'}_0$ than $\overline{w'\theta'}_{z_i}$, while $\alpha_{LH}$ and $\alpha_{F_c}$ decrease. Under fixed EZTG conditions, soil moisture-induced changes in $\alpha_{SH}$, $\alpha_{LH}$, and $\alpha_{F_c}$ range from 8.9% to 30.1%, −49.0% to −29.3%, and −69.2% to −39.5%, respectively. Comparisons between EZTG-induced top-down processes and soil moisture-induced bottom-up processes, $\alpha_{LH}$, and $\alpha_{F_c}$. For $\alpha_{SH}$, a balance exists between top-down and bottom-up processes, while for $\alpha_{LH}$ and $\alpha_{F_c}$, the two processes often act in the same direction, making their relative contributions less distinct. The implications of changes in entrainment fluxes of scalars and $\alpha$ for variations in flux divergence and convergence are discussed next.

### 3.2. Failure of the CFLA in the ASL in the Free Convection Limit

This section quantitatively explores how EZTG influences the slopes of flux profiles (i.e., changes in flux divergence and convergence), leading to varying degrees of failure in the CFLA in the ASL as highlighted in Figures 1g, 1h, and 1i. The degree of flux divergence or convergence is reflected by how far $\alpha$ deviates from unity (Liu, Liu, Huang, et al., 2024). Specifically, flux divergence of $\overline{w'q'}$ and $\overline{w'C'}$ occurs when $\alpha_{LH}$ and $\alpha_{F_c}$ are sub-unity, whereas flux convergence occurs when $\alpha_{LH}$ and $\alpha_{F_c}$ exceed unity as represented by changes in the slopes of flux profiles. Under the three fixed soil moisture conditions, EZTG-induced changes in the slopes of $\overline{w'\theta'}$, $\overline{w'q'}$, and $\overline{w'C'}$ profiles range from −7.7% to 1.3%, −10,518% to 794%, and −1,381% to 79%, respectively. This reveals that changes in the EZTG substantially regulate the degrees of flux divergence and convergence, thereby influencing the degrees of the validity of the CFLA. Under fixed EZTG conditions, soil moisture-induced changes in the slopes of $\overline{w'\theta'}$, $\overline{w'q'}$, and $\overline{w'C'}$ profiles range from 64% to 80%, −146% to 1,481%, and −402% to −95%, respectively. Therefore, soil moisture-induced changes in surface energy partitioning alter EZTG-induced entrainment processes, significantly contributing to changes in the slopes of the flux profiles and the degrees of the validity of the CFLA in the ASL. Comparisons between EZTG-induced and soil moisture-induced changes in the slopes indicate that variability in flux divergence of $\overline{w'\theta'}$ is more sensitive to changes in bottom-up processes than changes in top-down processes. However, variability in flux divergence and convergence for $\overline{w'q'}$ and $\overline{w'C'}$ is more sensitive to changes in top-down processes, or their sensitivities are comparable.

The distinct behaviors in flux divergence and convergence in $\overline{w'\theta'}$, $\overline{w'q'}$, and $\overline{w'C'}$ (i.e., differences in slopes even under the same conditions) indicate that flux divergence and convergence for $\overline{w'\theta'}$, $\overline{w'q'}$, and $\overline{w'C'}$ are not necessarily proportional (Figure 1g vs. Figure 1h vs. Figure 1i). Field data have shown that heat flux divergence is not directly associated with momentum flux divergence (Fairall et al., 2006; Mahrt et al., 2021; Ortiz-Suslow et al., 2021). Our findings, covering a wide range of soil moisture and EZTG conditions, reveal that the CFLA for $\overline{w'\theta'}$ is largely violated under wet soil moisture and weak to moderate EZTG conditions. Meanwhile, for $\overline{w'q'}$ and $\overline{w'C'}$, the CFLA is more significantly violated under dry soil moisture and weak to moderate EZTG conditions (i.e., flux convergence cases) and under wet soil moisture and strong EZTG conditions (i.e., flux divergence cases). Variations in $\alpha$ further imply that variability in divergence of $\overline{w'\theta'}$ is more sensitive to EZTG

changes under dry soil conditions, while variability in divergence/convergence of $\overline{w'q'}$ and $\overline{w'C'}$ is more sensitive to EZTG changes under wet soil conditions. In summary, variations in top-down scalar fluxes induced by EZTG changes regulate flux divergence and convergence of scalars in the ASL, contributing to different degrees of failure of the CFLA.

### 3.3. EZTG-Induced Energy Balance Non-Closure

Eddy covariance fluxes are often considered underestimated and overestimated if measured fluxes at any height in the ASL (i.e., $\overline{w'\theta'}(z)$, $\overline{w'q'}(z)$, and $\overline{w'C'}(z)$) are less and greater than their corresponding surface interfacial fluxes (i.e., $\overline{w'\theta'}_0$, $\overline{w'q'}_0$, and $\overline{w'C'}_0$), respectively. How EZTG-induced variations in underestimated *SH* and underestimated/overestimated *LH* in the ASL affect the non-closure is now explored considering the varying degrees of failure of the CFLA. Note that all fluxes are horizontally averaged across the domain, and the energy balance is guaranteed by the land-surface module at the surface-atmosphere interface.

Under each $f_n$ category, *CR* decreases significantly with increasing EZTG, mainly due to a decrease in *LH* (Figure 1j). *CR* can exceed unity for weak EZTG cases, such as EZweak-D, EZweak-M, EZweak-W, and EZmoderate-D, due to *LH* flux convergence (i.e., overestimated *LH*). Conversely, *CR* is less than 1 for cases with moderate to strong EZTG conditions with *LH* flux divergence. For cases with $CR > 1$, *CR* can increase with increasing height, or vice versa (Figure 1j). For each soil moisture condition, changes in $SH/(SH_0 + LH_0)$ are small, but $LH/(SH_0 + LH_0)$ varies substantially as EZTG decreases. For instance, $SH/(SH_0 + LH_0)$ at 40 m is 0.62, 0.63, and 0.63, and $LH/(SH_0 + LH_0)$ at 40 m is 0.41, 0.38, and 0.34 for EZweak-D, EZmoderate-D, and EZstrong-D, respectively (Figures 1k and 1l). These results suggest that larger variability in *LH* flux divergence/convergence than *SH* divergence in response to changes in top-down processes may be a major mechanism contributing to varying non-closure observed across global EC flux sites.

Furthermore, *CR* at $z = 40$ m under each fixed soil moisture condition shows substantial spatial variability, with values reaching as high as six at some locations. This spatial variability changes with EZTG (Figure 2) and is associated with the spatial variability in *LH* more than *SH* (Figures S6, S7 in Supporting Information S1). Prominent peaks with $CR > 1$ are present; for small EZTG, the overestimated *LH* primarily contributes to these peaks, while for large EZTG, the overestimated *SH* dominate (Figures S6, S7 in Supporting Information S1). These results highlight that spatial variability in EZTG-induced change in *SH* and *LH* in the ASL significantly contributes to the *CR*, even over homogeneous landscapes. This spatial heterogeneity is significant because of its practical consequences to EC scalar flux measurements. Flux towers, which provide point measurements, cannot capture simultaneous spatial and temporal averages of scalar fluxes. This limitation has two practical implications. First, the averaging period required to ensure that the temporal derivative of the vertical gradient of a scalar (i.e., $\frac{\partial}{\partial t}\left(\frac{\partial \overline{S}}{\partial z}\right) = 0$) is significantly longer than typical EC averaging times, necessitating a longer period to sample enough turbulent eddies and cancel transient effects. Second, limited sampling durations (e.g., 30 min to 1 hr) truncate the local co-spectrum, introducing biases that reduce turbulent flux measurements. This truncation affects flux gradient estimations differently across height, making them sensitive to the averaging interval. These factors together exacerbate challenges in flux measurements, highlighting a need for future studies on time-averaging versus ensemble-averaging under different entrainment conditions.

Previously, non-closure seemed to imply that both *SH* and *LH* are simultaneously underestimated compared to their true surface values. This is the reasoning underpinning the Bowen-ratio-preserving correction method (Twine et al., 2000), which allocates the energy balance residual to *SH* and *LH* by preserving $\beta$. This method assumes that $\beta$ is less impacted by the underestimation of *SH* and *LH* measured in the ASL. When the CFLA holds in the ASL, *SH* and *LH* remain constant with height, resulting in a height-invariant. Based on this premise, this method assumes that the EC-derived $\beta$ is robust. Using this $\beta$, along with net radiation and soil heat flux, the surface values of *SH* and *LH* can be inferred by this method. For this method to be valid, however, both *SH* and *LH* have to be proportionally underestimated. The work here shows that changes in $\beta_0$ are minimal across the three entrainment cases under each soil moisture regime, yielding mean $\beta$ values ($\overline{\beta_0}$) of 1.94 for dry soil, 0.90 for moderately dry soil, and 0.50 for wet soil (Table S2 in Supporting Information S1). These results indicate that even with the same $\overline{\beta_0}$ value under fixed soil moisture conditions, *CR* can exceed or fall below 1, indicating instances where *SH* is underestimated while *LH* is overestimated, even at the same $\beta_0$.

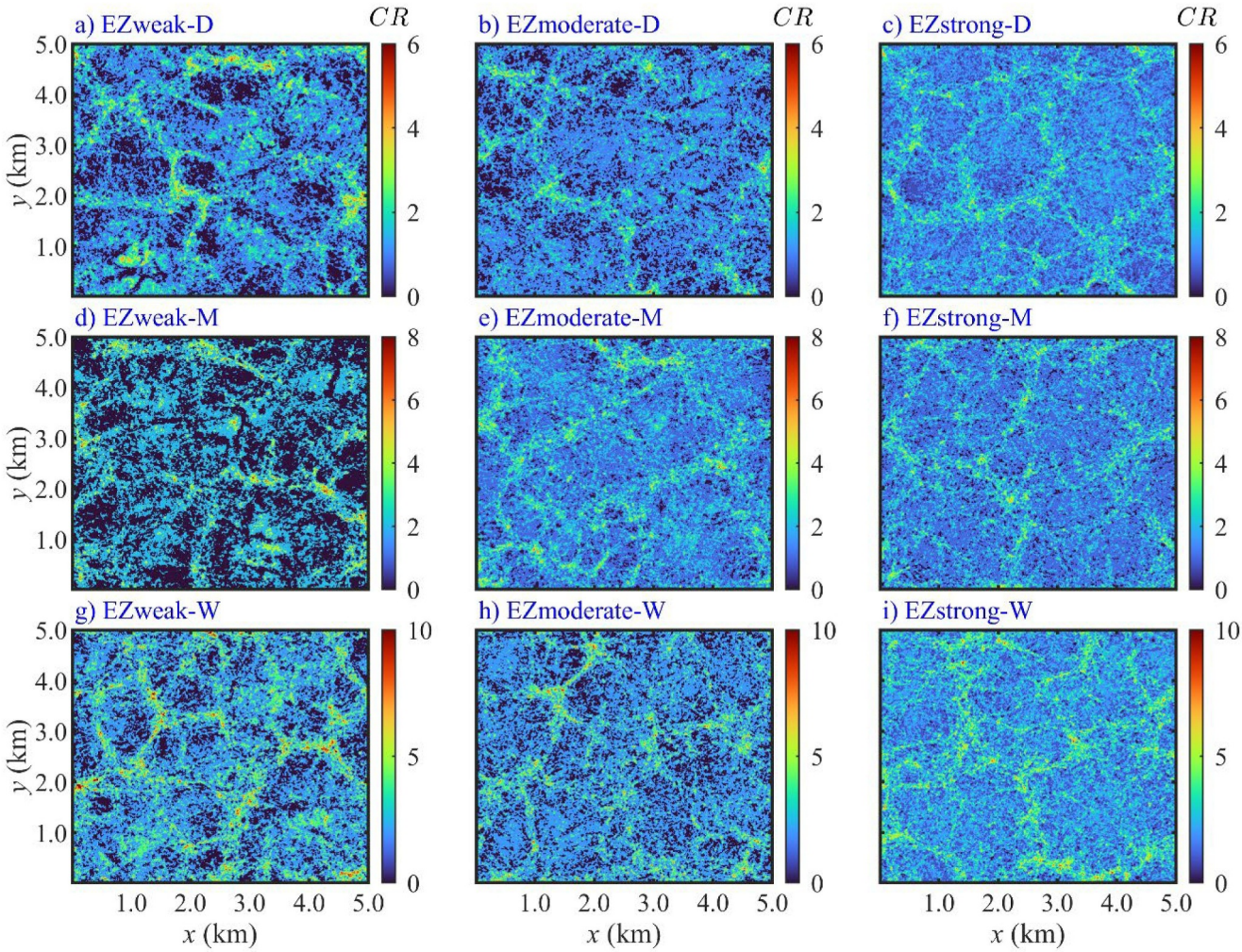


**Figure 2.** Horizontal ($x$–$y$) distributions of $CR$, defined as $CR = (SH + LH)/(SH_0 + LH_0)$, at $z = 40$ m for different cases.

When $CR < 1$, the positive residual ($res$) of the energy balance is distributed between $SH$ and $LH$ to obtain $SH_0 = SH + \Delta SH$ and $LH_0 = LH + \Delta LH$, where $\Delta SH = res \times x_a$ and $\Delta LH = res \times (1 - x_a)$ are positive and $x_a < 1$ is determined by preserving $\beta$ (i.e., $SH/LH = SH_0/LH_0$). However, this correction fails for the three cases with $CR < 1$ (i.e., EZmoderate-M, EZstrong-M, and EZmoderate-W), as adding a positive $\Delta LH$ to the already overestimated $LH$ leads to an artificially higher $LH_0$, while $SH_0$ is biased lower than expected by adding a smaller $\Delta SH$ to achieve the energy balance. For $CR > 1$, the negative residual ($res$) is partitioned into $SH$ and $LH$, based on the same practice. However, for $CR > 1$, adding a negative $\Delta SH$ to $SH$ leads to further underestimated $SH_0$ for the four cases (i.e., EZweak-D, EZmoderate-D, EZweak-M, and EZweak-W). These findings indicate that while the Bowen-ratio-preserving correction method may achieve surface energy balance closure, it does not guarantee accurate estimate of $SH_0$ and $LH_0$ in these cases. Moreover, it cannot be general and independent of the entrainment fluxes. EZTG-induced top-down processes substantially affect $CR$ by altering the degrees of $SH$ flux divergence and $LH$ flux convergence/divergence. Therefore, parameters related to entrainment processes should be included when developing methods to correct the flux imbalance.

Since large turbulent eddies are a primary mechanism for non-closure and the same large eddies carry heat and water vapor simultaneously, it was previously argued that both $SH$ and $LH$ in the ASL should be simultaneously underestimated in case of non-closure. However, it is now apparent that dissimilarity between heat and humidity flux transport is often observed under the influence of top-down large eddies (Gao et al., 2018, C. Liu, Liu, et al., 2021). Moreover, the increased $CR$ with an increasing $\beta$ is explained by overestimated $LH$ due to $LH$ flux convergence, despite $SH$ being underestimated (Liu, Liu, Huang, et al., 2024). Thus, both overestimated $LH$ and

underestimated *SH* can simultaneously occur in the ASL with the influence of the same large eddies, invalidating the Bowen-ratio-preserving correction method for proportionately adjusting *SH* and *LH* to achieve the closure.

The applicability of the Bowen-ratio-preserving correction method can be further assessed theoretically. The *CR* can be expressed as:

$$CR = \frac{SH_{EC} + LH_{EC}}{SH_0 + LH_0} = \frac{(SH_{EC}/LH_{EC} + 1)\, LH_{EC}}{(SH_0/LH_0 + 1)\, LH_0} = \frac{\beta_{EC} + 1}{\beta_0 + 1} \frac{LH_{EC}}{LH_0}, \tag{4}$$

where $SH_{EC}$ and $LH_{EC}$ are *SH* and *LH* measured by EC at a specific height in the ASL. The $\beta_{EC}$ and $\beta_0$ are the EC-derived and surface $\beta$, respectively. Substituting the relation $LH_{EC}/LH_0 = \overline{w'q'}/\overline{w'q'}_0$ from Equation 3 into Equation 4 yields:

$$CR = \frac{\beta_{EC} + 1}{\beta_0 + 1}\left(1 + (\alpha_{LH} - 1)\, \frac{z}{z_i}\right). \tag{5}$$

This equation indicates that *CR* is influenced by the variability of $\alpha_{LH}$, highlighting the significant role of boundary layer processes in regulating *CR*. The influence of the variability of $\alpha_{SH}$ on *CR* is embedded in $\beta_{EC}$, which itself is a function of *SH*. However, forcing $\beta_{EC} = \beta_0$ in Equation 5, as suggested by the Bowen-ratio-preserving correction method, assumes that *CR* depends solely on $\alpha_{LH}$. This assumption is fundamentally inaccurate since it neglects the impact of the typically underestimated *SH* on *CR*. Further, correcting $SH_{EC}$ and $LH_{EC}$ to achieve closure by making $CR = 1$ in Equation 5 yields:

$$\beta_0 = \beta_{EC} + \left(\beta_{EC} + 1\right)(\alpha_{LH} - 1)\, \frac{z}{z_i}. \tag{6}$$

Equation 6 demonstrates that $\beta_0 \neq \beta_{EC}$ under $CR = 1$ due to the influence of the availability of $\alpha_{LH}$ as long as $\alpha_{LH} \neq 1$. However, the condition $\beta_0 = \beta_{EC}$ under $CR = 1$ holds only when $\alpha_{LH} = 1$, which is rare since $\alpha_{LH} = 1$ leads to $\alpha_{SH} = 1$ under $\beta_0 = \beta_{EC}$ in the ASL. That means that both *SH* and *LH* should meet the CFLA simultaneously. Taking the ratio of $\beta_{EC}$ and $\beta_0$ and then incorporating the relations from Equation 3 for *SH* and *LH* gives:

$$\frac{\beta_{EC}}{\beta_0} = \frac{\frac{SH_{EC}}{LH_{EC}}}{\frac{SH_0}{LH_0}} = \frac{\frac{SH_{EC}}{SH_0}}{\frac{LH_{EC}}{LH_0}} = \frac{1 + (\alpha_{SH} - 1)\, \frac{z}{z_i}}{1 + (\alpha_{LH} - 1)\, \frac{z}{z_i}}. \tag{7}$$

Equation 7 indicates that $\beta_0 = \beta_{EC}$ holds only when $\alpha_{SH} = \alpha_{LH}$, a condition necessary for the Bowen-ratio-preserving correction method to perform as intended and a scenario in which the method may yield better results (Zhou et al., 2023). Therefore, the proposed theoretical arguments here reveal that the validity of the Bowen-ratio-preserving correction method is limited to situations where $\alpha_{SH}$ and $\alpha_{LH}$ are nearly equal, a condition not typically met particularly under convective atmospheric states.

## 4. Conclusions

The LES results of steady-state CBL flows indicate that changes in EZTG significantly regulate the linear dependency of scalar flux profiles with height over a horizontally homogeneous grass landscape with varying soil moisture levels. As the EZTG decreases, the entrainment fluxes for all scalars increase primarily due to increased entrainment velocity, leading to increased asymmetric scalar flux contributions between top-down and bottom-up transport. These changes in asymmetry alter the slopes of scalar flux profiles and the degrees of flux divergence and convergence in the ASL, contributing to varying degrees of failure in the CFLA.

Larger variations in the degrees of flux divergence for *SH* occur under drier soil conditions, mainly due to a combined effect of EZTG-induced changes in the boundary-layer height and top-down heat fluxes. In contrast, larger variations in the degrees of flux divergence/convergence for *LH* and $F_c$ occur under wetter soil conditions, as their top-down fluxes are more sensitive to EZTG variability.

Eddy covariance fluxes in the ASL are underestimated or overestimated when flux divergence or convergence occur, respectively, compared to the "true" surface fluxes. Therefore, EZTG-induced variations in flux divergence and convergence in the ASL regulate the degrees of the non-closure. *CR* is less than unity under strong EZTG conditions across all the soil moisture levels but can exceed unity under weak EZTG, especially with drier soil, where larger EZTG-induced top-down *LH* variations lead to greater variability in flux divergence/convergence of *LH*. The LES results suggest that large site-to-site variations in *CR* across global EC sites may be associated with greater variations in the degrees of flux divergence/convergence for *LH* more than flux divergence for *SH* or associated with the violation of the CFLA for *LH* more than for *SH*. Additionally, flux divergence and convergence for $F_c$ experience the largest variations in response to the greatest variabilities in EZTG-induced entrainment $CO_2$ fluxes compared to *SH* and *LH*. This suggests that $F_c$ measured by EC systems at flux sites may be subject to more significant underestimation or overestimation due to the influence of boundary-layer processes. Notably, unlike temperature, $\Delta_{EZ}s$ for $CO_2$ (and to a lesser extent, water vapor) may be positive or negative depending on the level of $CO_2$ concentrations in the free atmosphere. When $\alpha < 0$, deviations from a CFLA can be substantial. This study highlights the emerging need to quantify the influence of entrainment processes at the top of the boundary layer on flux divergence and convergence in the ASL. Entrainment may hold the key to interpreting EC fluxes, addressing the non-closure issue, and evaluating EC derived carbon balances. Additionally, over complex terrain covered by forest canopies, features such as downwind recirculation zones in sloping terrain, influenced by canopy-induced pressure gradients, advection, and drag, create spatial variability in flow patterns and scalar exchanges. These processes likely contribute to varying degrees of non-closure, highlighting the need for future studies to explore their impacts in heterogeneous landscapes.

## Data Availability Statement

According to the AGU publications Data Policy, the data used in this paper are deposited at Zenodo (Liu, Liu, Zhou, et al., 2024).

**Acknowledgments**
H. Liu acknowledges support from NSF-AGS-2325687 and NSF-AGS-1853050. C. Liu acknowledges support from National Natural Science Foundation of China (42105088). A. R. Desai acknowledges support from NSF-2313772. G. G. Katul acknowledges support from NSF-AGS-2028644 and Department of Energy (DE-SC0022072).

## References

Andre, I.-C., De Moor, G., Lacarrère, P., Therry, G., & du Vachat, R. (1978). Modeling the 24-hour evolution of the mean and turbulent structures of the planetary boundary layer. *Journal of the Atmospheric Sciences*, *35*(10), 1861–1883. https://doi.org/10.1175/1520-0469(1978)035<1861:mtheot>2.0.co;2

Butterworth, B. J., Desai, A. R., Metzger, S., Townsend, P. A., Schwartz, M. D., Bertram, T. H., et al. (2021). Connecting land-atmosphere interactions to surface heterogeneity in CHEESEHEAD19. *Bulletin of the American Meteorological Society*, *102*(2), E421–E445. https://doi.org/10.1175/BAMS-D-19-0346.1

Cancelli, D. M., Chamecki, M., & Dias, N. L. (2014). A large-eddy simulation study of scalar dissimilarity in the convective atmospheric boundary layer. *Journal of the Atmospheric Sciences*, *71*(1), 3–15. https://doi.org/10.1175/JAS-D-13-0113.1

Cava, D., Katul, G. G., Scrimieri, A., Poggi, D., Cescatti, A., & Giostra, U. (2006). Buoyancy and the sensible heat flux budget within dense canopies. *Boundary-Layer Meteorology*, *118*(1), 217–240. https://doi.org/10.1007/s10546-005-4736-1

Conzemius, R. J., & Fedorovich, E. (2006). Dynamics of sheared convective boundary layer entrainment. Part I: Methodological background and large-eddy simulations. *Journal of the Atmospheric Sciences*, *63*(4), 1151–1178. https://doi.org/10.1175/jas3691.1

Ek, M. B., & Holtslag, A. A. M. (2004). Influence of soil moisture on boundary layer cloud development. *Journal of Hydrometeorology*, *5*(1), 86–99. https://doi.org/10.1175/15257541(2004)005<0086:IOSMOB>2.0.CO;2

Fairall, C. W., Bariteau, L., Grachev, A. A., Hill, R. J., Wolfe, D. E., Brewer, W. A., et al. (2006). Turbulent bulk transfer coefficients and ozone deposition velocity in the international consortium for atmospheric research into transport and transformation. *Journal of Geophysical Research*, *111*(D23), D23S2. https://doi.org/10.1029/2006JD007597

Foken, T., Aubinet, M., Finnigan, J. J., Leclerc, M. Y., Mauder, M., & Paw U, K. T. (2011). Results of a panel discussion about the energy balance closure correction for trace gases. *Bulletin of the American Meteorological Society*, *92*(4), ES13–ES18. https://doi.org/10.1175/2011bams3130.1

Gao, Z., Liu, H., Katul, G. G., & Foken, T. (2017). Non-closure of the surface energy balance explained by phase difference between vertical velocity and scalars of large atmospheric eddies. *Environmental Research Letters*, *12*(3), 034025. https://doi.org/10.1088/1748-9326/aa625b

Gao, Z., Liu, H., Li, D., Katul, G. G., & Blanken, P. D. (2018). Enhanced temperature-humidity similarity caused by entrainment processes with increased wind shear. *Journal of Geophysical Research: Atmospheres*, *123*(8), 4110–4121. https://doi.org/10.1029/2017JD028195

Gao, Z., Liu, H., Russell, E. S., Huang, J., Foken, T., & Oncley, S. P. (2016). Large eddies modulating flux convergence and divergence in a disturbed unstable atmospheric surface layer. *Journal of Geophysical Research: Atmospheres*, *121*(4), 1475–1492. https://doi.org/10.1002/2015JD024529

Ghannam, K., Duman, T., Salesky, S. T., Chamecki, M., & Katul, G. G. (2017). The non-local character of turbulence asymmetry in the convective atmospheric boundary layer. *Quarterly Journal of the Royal Meteorological Society*, *143*(702), 494–507. https://doi.org/10.1002/qj.2937

Huang, J., Lee, X., & Patton, E. G. (2008). A modelling study of flux imbalance and the influence of entrainment in the convective boundary layer. *Boundary-Layer Meteorology*, *127*(2), 273–292. https://doi.org/10.1007/s10546-007-9254-x

Huang, J., Lee, X., & Patton, E. G. (2009). Dissimilarity of scalar transport in the convective boundary layer in inhomogeneous landscapes. *Boundary-Layer Meteorology*, *130*(3), 327–345. https://doi.org/10.1007/s10546-009-9356-8

Huang, J., Lee, X., & Patton, E. G. (2011). Entrainment and budgets of heat, water vapor, and carbon dioxide in a convective boundary layer driven by time-varying forcing. *Journal of Geophysical Research*, *116*(D6), D06308. https://doi.org/10.1029/2010JD014938

Katul, G., Kuhn, G., Schieldge, J., & Hsieh, C.-I. (1997). The ejection-sweep character of scalar fluxes in the unstable surface layer. *Boundary-Layer Meteorology*, *83*(1), 1–26. https://doi.org/10.1023/A:1000293516830

Khanna, S., & Brasseur, J. G. (1997). Analysis of Monin–Obukhov similarity from large-eddy simulation. *Journal of Fluid Mechanics*, *345*, 251–286. https://doi.org/10.1017/S0022112097006277

Lanotte, A. S., & Mazzitelli, I. M. (2013). Scalar turbulence in convective boundary layers by changing the entrainment flux. *Journal of the Atmospheric Sciences*, *70*(1), 248–265. https://doi.org/10.1175/jas-d-11-0330.1

Li, D., Katul, G. G., & Liu, H. (2018a). Intrinsic constraints on asymmetric turbulent transport of scalars within the constant flux layer of the lower atmosphere. *Geophysical Research Letters*, *45*(4), 2022–2030. https://doi.org/10.1002/2018GL077021

Li, Q., Gentine, P., Mellado, J. P., & Mccoll, K. A. (2018b). Implications of nonlocal transport and conditionally averaged statistics on Monin-Obukhov similarity theory and Townsend's attached eddy hypothesis. *Journal of the Atmospheric Sciences*, *75*(10), 3403–3431. https://doi.org/10.1175/JAS-D-17-0301.1

Liu, C., Liu, H., Huang, J., & Xiao, H. (2021). Varying partitioning of surface turbulent fluxes regulates temperature-humidity dissimilarity in the convective atmospheric boundary layer. *Geophysical Research Letters*, *48*(21), e2021GL095836. https://doi.org/10.1029/2021GL095836

Liu, H., Gao, Z., & Katul, G. G. (2021). Non-closure of surface energy balance linked to asymmetric turbulent transport of scalars by large eddies. *Journal of Geophysical Research: Atmospheres*, *126*(7), e2020JD034474. https://doi.org/10.1029/2020JD034474

Liu, H., Liu, C., Huang, J., Desai, A. R., Zhang, Q., Ghannam, K., & Katul, G. G. (2024). Scalar flux profiles in the unstable atmospheric surface layer under the influence of large eddies: Implications for eddy covariance flux measurements and the non-closure problem. *Geophysical Research Letters*, *51*(1), e2023GL106649. https://doi.org/10.1029/2023GL106649

Liu, H., Liu, C., Zhou, Y., Zhang, Q., Desai, A., Ghannam, K., et al. (2024). Is there a scalar atmospheric surface layer within a convective boundary layer? Implications for flux measurements. *Zenodo*. [Dataset]. https://doi.org/10.5281/zenodo.13767777

Mahrt, L., Nilsson, E., Rutgersson, A., & Pettersson, H. (2021). Vertical divergence of the atmospheric momentum flux near the sea surface at a coastal site. *Journal of Physical Oceanography*, *51*(11), 3529–3537. https://doi.org/10.1175/jpo-d-21-0081.1

Mauder, M., Foken, T., & Cuxart, J. (2020). Surface-energy-balance closure over land: A review. *Boundary-Layer Meteorology*, *9*(8), 1–32. https://doi.org/10.1007/s10546-020-00529-6

Mellado, J., Puche, P. M., & van Heerwaarden, C. C. (2017). Moisture statistics in free convective boundary layers growing into linearly stratified atmospheres. *Quarterly Journal of the Royal Meteorological Society*, *143*(707), 2019–2403. https://doi.org/10.1002/qj.3095

Moeng, C. H. (1984). A large-eddy-simulation model for the study of planetary boundary-layer turbulence. *Journal of the Atmospheric Sciences*, *41*(13), 2052–2062. https://doi.org/10.1175/1520-0469(1984)041<2052:ALESMF>2.0.CO;2

Oncley, S., Foken, T., Vogt, R., Kohsiek, W., DeBruin, H. A. R., Bernhofer, C., et al. (2007). The energy balance experiment EBEX-2000. Part I: Overview and energy balance. *Boundary-Layer Meteorology*, *123*(1), 1–28. https://doi.org/10.1007/s10546-007-9161-1

Ortiz-Suslow, D. G., Kalogiros, J., Yamaguchi, R., & Wang, Q. (2021). An evaluation of the constant flux layer in the atmospheric flow above the wavy air-sea interface. *Journal of Geophysical Research: Atmospheres*, *126*(8), e2020JD032834. https://doi.org/10.1029/2020JD032834

Patton, E. G., Sullivan, P. P., & Moeng, C. H. (2005). The influence of idealized heterogeneity on wet and dry planetary boundary layers coupled to the land surface. *Journal of the Atmospheric Sciences*, *62*(7), 2078–2097. https://doi.org/10.1175/JAS3465.1

Sorbjan, Z. (1999). Similarity of scalar fields in the convective boundary layer. *Journal of the Atmospheric Sciences*, *56*(13), 2212–2221. https://doi.org/10.1175/1520-0469(1999)056<2212:sosfit>2.0.co;2

Sorbjan, Z. (2005). Statistics of scalar fields in the atmospheric boundary layer based on large-eddy simulations. Part I: Free convection. *Boundary-Layer Meteorology*, *116*(3), 467–486. https://doi.org/10.1007/s10546-005-0907-3

Stoy, P. C., Mauder, M., Foken, T., Marcolla, B., Boegh, E., Ibrom, A., et al. (2013). A data-driven analysis of energy balance closure across FLUXNET research sites: The role of landscape scale heterogeneity. *Agricultural and Forest Meteorology*, *171–172*, 137–152. https://doi.org/10.1016/j.agrformet.2012.11.004

Stull, R. B. (1988). *An introduction to boundary layer meteorology*. Kluwer Academic Publishers.

Sullivan, P. P., McWilliams, J. C., & Moeng, C. H. (1996). A grid nesting method for large-eddy simulation of planetary boundary-layer flows. *Boundary-Layer Meteorology*, *80*(1), 167–202. https://doi.org/10.1007/BF00119016

Twine, T. E., Kustas, W. P., Norman, J. M., Cook, D. R., Houser, P., Meyers, T. P., et al. (2000). Correcting eddy-covariance flux underestimates over a grassland. *Agricultural and Forest Meteorology*, *103*(3), 279–300. https://doi.org/10.1016/s0168-1923(00)00123-4

Wanner, L., Jung, M., Paleri, S., Butterworth, B. J., Desai, A. R., Sühring, M., & Mauder, M. (2024). Towards energy-balance closure with a model of dispersive heat fluxes. *Boundary-Layer Meteorology*, *190*(5), 25. https://doi.org/10.1007/s10546-024-00868-8

Wyngaard, J. C. (1982). Lectures on the planetary boundary layer. In D. K. Lilly & T. Gal-Chen (Eds.), *Mesoscale meteorology—theory, observations and models* (pp. 603–650). D. Reidel.

Wyngaard, J. C. (1990). Scalar fluxes in the planetary boundary layer—Theory, modeling, and measurement. *Boundary-Layer Meteorology*, *50*(1–4), 49–75. https://doi.org/10.1007/bf00120518

Wyngaard, J. C. (2010). *Turbulence in the atmosphere*. Cambridge University Press.

Wyngaard, J. C., & Brost, R. A. (1984). Top-down and bottom-up diffusion of a scalar in the convective boundary layer. *Journal of the Atmospheric Sciences*, *41*(1), 102–112. https://doi.org/10.1175/1520-0469(1984)041<0102:TDABUD>2.0.CO;2

Zhou, Y., Li, D., Liu, H., & Li, X. (2018). Diurnal variations of the flux imbalance over homogeneous and heterogeneous landscapes. *Boundary-Layer Meteorology*, *168*(3), 1–26. https://doi.org/10.1007/s10546-018-0358-2

Zhou, Y., Sühring, M., & Li, X. (2023). Evaluation of energy balance closure adjustment and imbalance prediction methods in the convective boundary layer – a large eddy simulation study. *Agricultural and Forest Meteorology*, *333*, 109382. https://doi.org/10.1016/j.agrformet.2023.109382